

# Simulating the photoelectron spectra of rare-gas clusters

François G. Amar,<sup>a)</sup> James Smaby, and Thomas J. Preston  
*Department of Chemistry, University of Maine, Orono, Maine 04469-5706*

(Received 2 March 2005; accepted 21 April 2005; published online 5 July 2005)

Motivated by the recent experiments of the Swedish group [M. Tchapyguine, R. R. Marinho, M. Gisselbrecht *et al.*, *J. Chem. Phys.* **120**, 345 (2004)], we simulate the photoelectron spectra of pure xenon and argon clusters. The clusters are modeled using molecular dynamics with Hartree–Fock–dispersion type pair potentials while the spectrum is calculated as the sum of final state energy shifts of the atoms ionized within the cluster relative to the isolated gas phase ion. A self-consistent polarization formalism is used. Since signal electrons must travel through the cluster to reach the detector, we have accounted for the attenuation of the signal intensity by integrating an exponentially decaying scattering expression over the geometry of the cluster. Several different approaches to determining the required electron mean free paths (as a function of electron kinetic energy) are considered. Our simulated spectra are compared to the experimental results. © 2005 American Institute of Physics. [DOI: 10.1063/1.1931527]

## I. INTRODUCTION

The problem of determining cluster structure, especially for neutral clusters which are generally not mass selected, is a difficult one that has occupied a number of groups for many years. Spectroscopic techniques have been applied to guest-host systems in which a chromophore acts as a probe of cluster structure,<sup>1</sup> however, the guest molecules can have a severe perturbing influence on the structure itself.<sup>2</sup> For neat clusters of rare gases, there are relatively few “handles” by which to probe the structure of the cluster. Notable work in this area includes the electron diffraction experiments of the Farges group on rare gas and molecular clusters.<sup>3,4</sup> Simulation has played a significant role in helping to construct models whose radial distribution functions are Fourier transformed for comparison with experimental diffraction patterns. On the theoretical side, systematic attempts to find global (and higher-lying local) minimum structures for Lennard-Jones systems<sup>5–8</sup> have helped to create a map of the rough energy landscape of rare-gas clusters.<sup>9,10</sup> The combined efforts of theory and experiment have resulted in a fairly nuanced picture of the transformation of rare-gas clusters, e.g., argon, through a variety of structural motifs with increasing size: from polyicosahedral ( $19 < N < 100$ ) to multishell icosahedral ( $100 < N < 750$ ) to decahedral ( $10^3 < N < 2 \times 10^5$ ) and finally to “bulk” ordering or fcc ( $N > 2 \times 10^5$ ).<sup>11</sup>

Recent work by the Swedish group<sup>12</sup> has provided a new tool for looking at neutral rare-gas cluster structure in the form of core-level x-ray photoelectron spectroscopy. The present study is motivated, in particular, by the work presented by Tchapyguine *et al.*<sup>13</sup> on pure rare-gas clusters and by the extension of that work to mixed clusters (e.g.,

Xe/Ar).<sup>14,15</sup> In the present investigation we focus on simulating the photoelectron spectra of pure Xe and Ar clusters. Our work on mixed clusters will be the subject of a future publication. We discuss our simulation methodology in the following section and then present and discuss our results.

## II. SIMULATION METHODOLOGY

### A. Interaction potentials

We model the mixed rare-gas clusters with high quality pair potentials of the Hartree–Fock–dispersion (HFD)-type pioneered by Aziz and co-workers.<sup>16</sup> We use the HFD-B2 Xe–Xe potential of Dham *et al.*<sup>17</sup> and the HFD-C Ar–Ar potential of Aziz and Chen:<sup>18</sup>

$$V_{\text{HFD-B2}} = \varepsilon \left[ A e^{-\alpha r + \beta r^2} - F \sum_{i=0}^2 \frac{C_{2i+6}}{r^{2i+6}} \right],$$

$$V_{\text{HFD-C}} = \varepsilon \left[ A r^\gamma e^{-\alpha r} - F \sum_{i=0}^2 \frac{C_{2i+6}}{r^{2i+6}} \right],$$

where

$$F = \begin{cases} 1, & r \geq D \\ e^{-(D/r-1)^2}, & r < D \end{cases} \quad (1)$$

Here  $r$  is a reduced distance  $R/R_e$ , and all other parameters are thus dimensionless, with the exception of  $\varepsilon$ , the bond dissociation energy, given in the desired energy unit. While we do not detail the nine or so parameters required for each potential here, we do give the equilibrium distance and dissociation energies for each dimer pair in Table I.

### B. Cluster formation and equilibration

In order to generate and equilibrate clusters of a given size, we have started from the set of “spherical” clusters

<sup>a)</sup>Author to whom correspondence should be addressed; Electronic mail: amar@maine.edu

TABLE I. Equilibrium bond distances and well depths for the rare-gas pair potentials used in this work.

Dimer	$R_e$ (Å)	$\epsilon$ (K)
Ar–Ar <sup>a</sup>	3.759	143.224
Xe–Xe <sup>b</sup>	4.3656	282.8

<sup>a</sup>HFD-C potential of Aziz *et al.* (Ref. 18).<sup>b</sup>HFD-B2 potential of Dham *et al.* (Ref. 17).

discussed by Abraham which are based on a close-packed scheme.<sup>19</sup> The clusters are then thermalized by molecular dynamics (MD) inside a hard-wall bounding sphere. We used a discrete annealing procedure, running each cluster trajectory at five different temperatures for definite amounts of time<sup>20</sup> before using a conjugate gradient quenching algorithm<sup>21</sup> to bring the cluster to a local minimum on the potential hypersurface. The initial temperatures were chosen rather high to minimize the amount of time needed to introduce substantial disorder into the clusters while the final temperature is close to the typical melting temperature for small rare-gas clusters. The bounding sphere's volume was diminished linearly by a factor of 2 as the temperature was lowered.

### C. Spectral shift calculation

Under the assumption of very fast escape of the signal electron, with no possibility of nuclear motion, and neglecting electronic reorganization, we model the change in the binding energy of the core hole ( $4d_{5/2}$  for Xe and  $2p_{3/2}$  for Ar) relative to the isolated atom by computing the polarization energy of the ionized atom in its cluster environment with the neutral cluster geometry. The charge is treated as a point charge while the cluster atoms (including the ionized atom) are modeled with point polarizability  $\alpha$ , with values  $1.6411 \text{ \AA}^3$  and  $4.044 \text{ \AA}^3$  for Ar and Xe respectively.<sup>22</sup> The calculation is performed self-consistently as follows:<sup>23</sup> first, induced dipoles are created on all the atoms by the electric field of the ion,

$$\boldsymbol{\mu}_i = \alpha_i \mathbf{E}_i = \alpha_i \left[ \mathbf{E}_i^{\text{coul}} - \sum_{j=1}^n \mathbf{T}_{ij} \cdot \boldsymbol{\mu}_j \right], \quad i = 1, n, \quad (2)$$

where the components  $\mathbf{T}_{ij}$  of the dipole-dipole interaction tensor are given by

$$\mathbf{T}_{ij} = \left[ \mathbf{I} - \frac{3\mathbf{r}_{ij}\mathbf{r}_{ij}}{r_{ij}^2} \right] \frac{1}{r_{ij}^3}. \quad (3)$$

Now  $\mathbf{E}_i^{\text{coul}} = e\mathbf{r}_{ij}/r_{ij}^3$  but  $\mathbf{E}_i$  depends on the  $\boldsymbol{\mu}_j$ , so we must iterate Eq. (2) to self-consistency. The polarization energy is then calculated<sup>24,25</sup> as

$$E_{\text{ion}} = -e \sum_{i=1}^n \sum_{j=1}^n \frac{\boldsymbol{\mu}_j \cdot \mathbf{r}_{ij}}{r_{ij}^3} + \sum_{i<j} \boldsymbol{\mu}_i \cdot \mathbf{T}_{ij} \cdot \boldsymbol{\mu}_j + \sum_{i=1}^n \frac{\boldsymbol{\mu}_i \cdot \boldsymbol{\mu}_i}{2\alpha_i}. \quad (4)$$

For our calculations it takes between six and eight iterations to converge the polarization energy to 1 part in  $10^6$ . No distance cutoffs are used.

To construct the photoelectron spectrum, we perform the calculation just described with each atom of a cluster taking the role of the ion and then we bin the distribution of energies so obtained. In order to compare the binding energy shift that we calculate directly with experiment, we must add the appropriate binding energy for the relevant free atom state: 248.4 eV for the Ar  $2p_{3/2}$  state and 67.5 eV for the Xe  $4d_{5/2}$  state.<sup>13</sup> In practice, for clusters of the order of 1000 atoms, we typically use an ensemble of about five clusters, each independently equilibrated to improve the signal-to-noise ratio of the simulated spectrum. The raw polarization data must then be treated to compensate for signal attenuation due to scattering processes and, finally, broadened with an experimental line shape function.

### D. Signal attenuation

The distribution of final state energies [computed using Eq. (4)] over the ensemble of atoms in a cluster is not directly measurable since electron scattering effects attenuate the electron signal. This attenuation is due to inelastic and possibly elastic scattering processes and is a function of the material, the distance traveled, and the kinetic energy of the electron.

The Swedish group has been careful to make a series of measurements at photon energies that yield electron kinetic energy that are similar for both Xe and Ar spectra in both the pure and mixed clusters. For example, a photon of energy 120 eV ejects a Xe  $4d_{5/2}$  electron (from the isolated atom) with a kinetic energy of 52.5 eV for a binding energy of 67.5 eV. For the Ar  $2p_{3/2}$  core hole, with binding energy of about 248.4 eV, a photon of energy  $\sim 298$  eV is required to generate electrons with a kinetic energy of 50 eV. The argon cluster experiments reported in Ref. 13 were carried out with a photon energy of 310 eV yielding signal electrons of about 60 eV kinetic energy. Since the maximal shift of binding energy due to cluster polarization effects is of the order of 0.5–1.5 eV, we are justified in treating the attenuation parameter as a constant for fixed photon energy.

### E. Attenuation model

We have constructed a model for treating the effect of the cluster geometry on the signal attenuation. As shown by the Swedish group, electrons traveling from the center of a cluster must traverse, on average, a larger distance through the scattering medium and thus proportionally fewer of these “bulklike” electrons are detected than those originating at or near the surface of the cluster. Figure 1 shows a schematic of a cluster, treated as a sphere of radius  $R$ ; the position  $r$  of an ionized atom  $A$  is shown relative to the center of mass  $C$  of the cluster. Because a given cluster has a random orientation

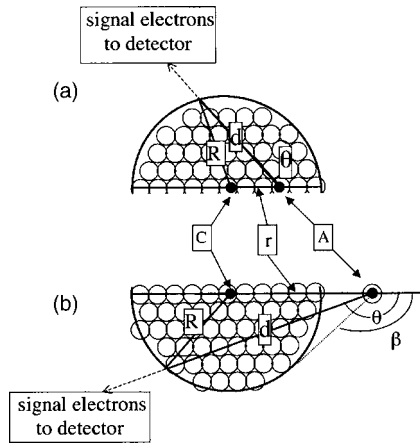


FIG. 1. Schematic of orientational averaging procedure of Eqs. (8) and (9) for nearly spherical clusters: (a)  $r < R$ ; (b)  $r > R$ .

with respect to the detector, the signal electron coming from a given ion could be emitted in any direction relative to an axis system fixed in the cluster. Within a spherical cluster approximation, the vector from the center of mass to the ion acts as an axis of cylindrical symmetry and so the only non-trivial integration is that over the angle  $\theta$ . This analysis can be expressed as follows. The probability that an electron will reach, unscattered, a distance  $d$  through a uniform medium is

$$P = e^{-d/\lambda}, \quad (5)$$

where  $\lambda$  is an effective mean free path. For  $r \leq R$ , to determine  $d$  for a given value of  $\theta$ , apply the law of cosines,

$$R^2 = d^2 + r^2 - 2rd \cos \theta. \quad (6)$$

Using the quadratic formula to solve for  $d$ ,

$$\begin{aligned} d &= \frac{1}{2}(2r \cos \theta \pm \sqrt{4r^2 \cos^2 \theta - 4(r^2 - R^2)}) \\ &= r \cos \theta \pm \sqrt{r^2 \cos^2 \theta + R^2 - r^2}, \end{aligned} \quad (7)$$

we choose the positive root. We get the total probability of detecting an electron from a given ionic position *inside* the cluster by integrating over  $\theta$ :

$$\begin{aligned} \langle P \rangle &= \frac{1}{\pi} \int_0^\pi e^{-d(\theta)/\lambda} d\theta \\ &= \frac{1}{\pi} \int_0^\pi e^{-(r \cos \theta + \sqrt{r^2 \cos^2 \theta + R^2 - r^2})/\lambda} d\theta. \end{aligned} \quad (8)$$

For atoms that are at the surface and just outside of radius that we determine for each model cluster, a similar analysis to the one above yields, for  $r > R$ ,

$$\langle P \rangle = \frac{1}{\pi} \left\{ \int_0^\beta d\theta + \int_\beta^\pi e^{-(2\sqrt{r^2 \cos^2 \theta + R^2 - r^2})/\lambda} d\theta \right\} \quad (9a)$$

where

$$\beta = \arcsin(R/r). \quad (9b)$$

This attenuation model has two important differences from that presented by Tchapyguine *et al.*<sup>13</sup> First, this model is an atomic site model rather than a continuum layer model. Thus, as discussed above, we associate the signal from each

ion with a distinct polarization energy as calculated by Eq. (4). Second, this model is orientationally averaged since our relatively small number of annealed cluster models is intended to represent an ensemble of clusters in the beam and because the site model no longer has spherical symmetry.

Equations (8) and (9) contain two parameters:  $R$  which is determined from our cluster model and  $\lambda$  which must be obtained from experiment or independent theory. While our clusters do not have perfect spherical symmetry, the models are quite spherical, but, because of the thermal treatment, have rough surfaces. If we simply set the cluster radius to the distance of the outermost atom, we would certainly be overestimating  $R$  and thus overestimating the electron attenuation. We have looked at the radial distribution function of a number of clusters and determined that the inflection point in the number density at the cluster-gas boundary correlates well with the value of  $R$  that puts about 1/4 of the expected surface atoms of a given cluster outside the spherical boundary. Each cluster in an ensemble representing a given cluster of given size has a (slightly) different  $R$  value determined in this way.

## F. Attenuation parameters

We have considered two approaches to determining the scattering length parameter given in the model above. First we can use the data given in the paper by Tchapyguine *et al.*<sup>13</sup> For a given electron kinetic energy, these authors compare measured bulk-to-surface peak ratios for a given average cluster size with the predictions of their exponential decay model in order to determine the *effective escape depths* (their  $\lambda$  parameter) for both Xe and Ar clusters. They specifically calculate  $\lambda$  for Xe at 43 eV to be 14 Å. Using the data given in Figs. 9 and 2 of Ref. 13, we estimate  $\lambda(\text{Xe}, 50 \text{ eV}) = 17 \text{ Å}$  and  $\lambda(\text{Ar}, 50 \text{ eV}) = 9 \text{ Å}$ .

Our second approach is to turn to the literature on electron attenuation<sup>26</sup> and, in particular, to the empirical fitting model of Tanuma, Powell, and Penn,<sup>27</sup> the so-called TPP-2M model. This model has produced a successful correlation of the inelastic mean free path (IMFP) with several input parameters for a given material: density, atomic number, number of valence electrons, and energy gap. While the model has been applied more commonly to metals it has also been used for semiconductors and insulators. Table II gives the input data for Xe and Ar as well as the predicted IMFP for 50 eV electrons along with the escape depths of Tchapyguine. We have checked our coding of this formula against the QUASES-IMFP-TPP2M program available on the world wide web.<sup>28</sup> The energy gap parameters for Xe and Ar were taken from the paper of Baldini;<sup>29</sup> these values are corroborated by other authors.<sup>30</sup> IMFPs obtained in this way are generally considered good to about 20%.

We note that for 60 eV signal electrons, the TPP-2M formula predicts  $\lambda_{\text{Ar}} = 11.3 \text{ Å}$  (a bit less attenuation than at 50 eV); however, it is clear that for argon, the IMFP values calculated using the TPP-2M formula are in essential agreement (to within 20%) with the effective escape depths given in Ref. 13. For xenon, however, we see a significant dis-

TABLE II. Predicted attenuation lengths for 50 eV electrons in Ar and Xe clusters. IMFP refers to the inelastic mean free path values generated by the TPP-2M formula (Ref. 27) using the molar mass, material density, energy gap, and number of valence electrons as parameters. The column labeled EED refers to electron escape depths taken from the data in Ref. 13.

Rare gas	IMFP (Å)	EED (Å)	$M$ (g mol <sup>-1</sup> )	$\rho$ (g cm <sup>-3</sup> )	$E_g$ (eV)	$N_v$
Ar	11	9	39.95	3.655	14.3	8
Xe	6.5	17	131.29	1.65	9.28	8

agreement in the attenuation lengths taken from the TPP-2M formula or as determined by Tchapyguine *et al.*<sup>13</sup> As we shall see below, we are able to reproduce the experimental photoelectron spectra with our orientationally averaged atomic site polarization model, only if we use values for attenuation lengths that are close to those given by the TPP-2M formula.

### G. Broadening

We have used the line shape of the atomic signal from the experiments of the Swedish group as a broadening function for our simulated spectra. Voigt profiles<sup>31</sup> were used both for Xe and Ar, with Doppler and Lorentz widths kindly provided by Lundwall.<sup>32</sup> The Voigt function was convoluted with the polarization energy distribution obtained by applying Eq. (8) to the polarization calculations performed using Eq. (4).

## III. RESULTS

### A. Polarization histograms

We first present the results of our polarization calculations on a series of argon and xenon clusters of different sizes. Figure 2 displays the raw polarization shift data for clusters of Xe with  $150 \leq n \leq 1000$ . In both the xenon simulations of Fig. 2 and the corresponding polarization histograms for argon (not shown), we see the broad double maxi-

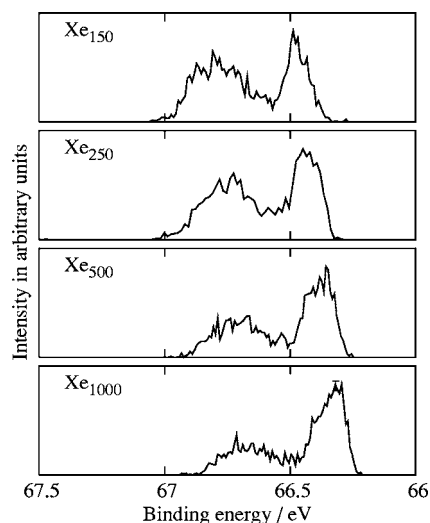


FIG. 2. Raw polarization energy histograms for Xe clusters for four sizes. The energy zero is shifted to the experimental value of the atomic Xe  $4d_{5/2}$  peak. The bulk peak shifts to lower binding energies with increasing size. Likewise, the bulk peak grows in size in accordance with the square-cube law. A typical uncertainty is shown on the Xe<sub>1000</sub> histogram.

um structure due to “surface” and bulklike environments with the latter shifted to lower binding energy. We also can see that as the clusters get larger, the relative intensity of the more shifted, bulklike peak increases in accord with the square-cube law. Finally we can see that the net shift of the bulk peak increases with size as would be expected when the amount of dielectric material increases.

### B. Simulated photoelectron spectra

Figure 3 illustrates the effect of broadening and attenuation on the “raw” histogram data in order to obtain simulated spectra that can be compared directly with experiment. Figure 3(a) is the raw polarization histogram for Xe<sub>309</sub>—initially a perfect cuboctahedron but then heated and annealed as described above. Figure 3(b) shows the convolution of the experimental Voigt line shape for atomic Xe with the data of Fig. 3(a), resulting in a highly smoothed, broadened spectrum whose bulk and surface peak heights are, however, unchanged. In Fig. 3(c) we have first applied the orientationally averaged attenuation procedure to the data of Fig. 3(a) and then broadened that result to obtain a final simulated spectrum. The attenuation length parameter was set to the value  $\lambda = 8.5$  Å for this figure. We note a dramatic

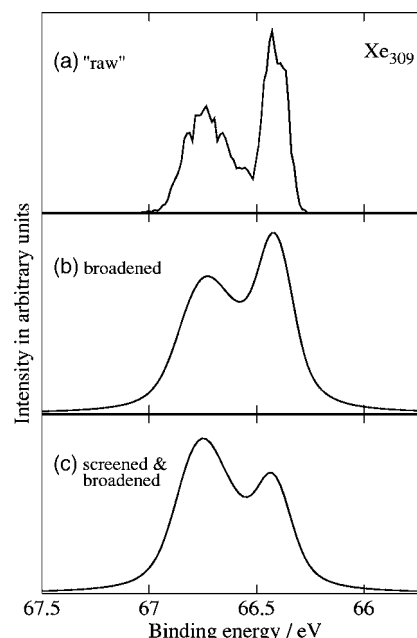


FIG. 3. Creation of a simulated spectrum (here Xe<sub>309</sub>) proceeds by generating a “raw” polarization energy histogram as in (a) In (b) the effect of broadening is displayed, while (c) displays the final spectrum that is both screened (with  $\lambda_{Xe} = 8.5$  Å) and broadened.

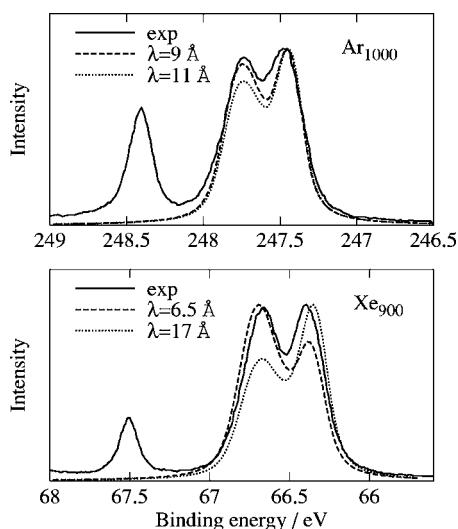


FIG. 4. Top panel: comparison of simulated Ar photoelectron spectra for two values of effective electron mean free path ( $\lambda_{\text{Ar}}=9 \text{ \AA}, 11 \text{ \AA}$ ) for  $\text{Ar}_{1000}$  with experimental argon spectrum for  $\langle N_{\text{Ar}} \rangle=1000$ . Bottom panel: comparison of simulated Xe photoelectron spectra ( $\lambda_{\text{Xe}}=6.5 \text{ \AA}, 17 \text{ \AA}$ ) for  $\text{Xe}_{900}$  with experimental xenon spectrum for  $\langle N_{\text{Xe}} \rangle=900$  (we used the Digitizeit program (Ref. 38) in order to replot data from Figs. 3 and 5 of Ref. 13). Plots are normalized to the experimental bulk peak.

decrease in the bulk signal intensity relative to the surface peak in going from Fig. 3(b) (no attenuation or  $\lambda \rightarrow \infty$ ) to Fig. 3(c).

### C. Attenuation parameters

It is clear that a key aspect of the comparison of our simulated spectra with the experimental data is the value of the attenuation length  $\lambda$ . Recall that for argon, the TPP-2M formula gave the same results as Ref. 13 (to within 20%) while for Xe, we must make a critical evaluation of the two disparate values for the  $\lambda$  parameter. In Fig. 4 (bottom panel), we compare the simulated spectra for  $\text{Xe}_{900}$  at two different values of the attenuation parameter with the experimental data, taken from Fig. 3 of Ref. 13 for Xe clusters of mean size  $\langle N \rangle=900$ . Here, starting with the same histogram data, the simulated spectra have  $\lambda_{\text{Xe}}=17 \text{ \AA}$  and  $6.5 \text{ \AA}$ . These two values of  $\lambda_{\text{Xe}}$  generate simulated spectra that bracket the experimental one. The top panel of Fig. 4 shows the results for similar calculations for argon clusters of 1000 atoms with  $\lambda_{\text{Ar}}$  equal to  $9 \text{ \AA}$  or  $11 \text{ \AA}$ . In this case the simulation results are less easily distinguished, confirming that 20% uncertainty in  $\lambda$  is at the limit of detection using the present techniques.

Once the histograms [e.g., Fig. 3(a)] have been generated for a particular cluster size/geometry, it is relatively easy to apply the attenuation model with a variety of attenuation lengths. We have thus attempted to determine the “best” values of  $\lambda_{\text{Xe}}$  and  $\lambda_{\text{Ar}}$  for 50 eV (60 eV for argon) signal electrons by comparing our simulated spectra with the spectra given in Figs. 3 and 5 of Ref. 13. We have computed the ratio of peak heights of bulk and surface peaks for experimental curves and for model clusters with sizes equal to the reported mean size  $\langle N \rangle$ . In the latter case we have systematically varied the attenuation parameter to generate different

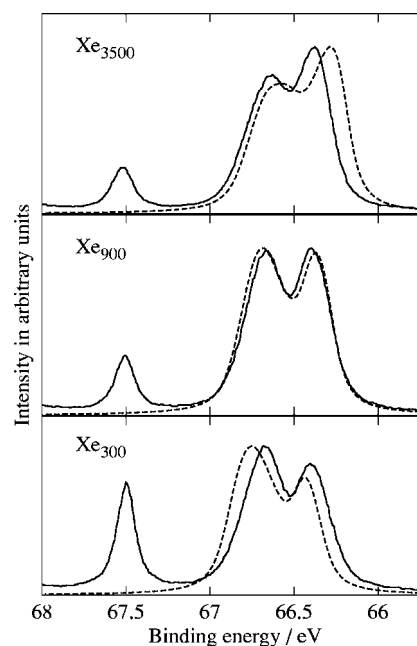


FIG. 5. Comparison of pure Xe ( $\langle N \rangle=300, 900, 3500$ ) experimental spectra with “best fit” simulated spectra ( $\lambda_{\text{Xe}}=8.5 \text{ \AA}$ ) using clusters of size equal to the mean size. Plots are normalized to the largest cluster peak.

spectra. We then compute the weighted sum of the squares of the difference of experimental and simulated bulk/surface peak height ratios (divided by the experimental ratios squared) in order to minimize this quantity over the full range of reported size data:  $\langle N \rangle_{\text{Xe}}=300, 900, 3500$  and  $\langle N \rangle_{\text{Ar}}=300, 1000, 3000$ . We note that other fitting schemes are possible, perhaps even preferable: for example, using integrated intensities under each peak by fitting the overall spectrum to a sum of elementary line shape functions (Voigt or Gaussian). The present scheme is simple and uses peak information in a manner similar to that reported in Ref. 13.

The results are shown in Figs. 5 and 6. We have plotted our simulated spectra for Xe and Ar on top of the experimental spectra using a single attenuation parameter for each species. The spectra are normalized to the highest peak in the experimental curves. For Xe, the attenuation parameter is  $\lambda_{\text{Xe}}=8.5 \text{ \AA}$  while  $\lambda_{\text{Ar}}=9.5 \text{ \AA}$ . In determining these values, we have given more weight to the larger clusters. As intimated above, the argon result is consistent with both of the earlier estimates of attenuation parameters described in Sec. II. However, for xenon, the large value of  $\lambda$  reported by the Swedish group appears to be inconsistent with our findings, which are, of course, based on a more detailed model of the cluster spectrum. Note that for smaller clusters, we do not quite recover the full shift that is seen in the experiment while for large Xe clusters our simulated spectra appears to overestimate the shift. This will be discussed further below.

### IV. DISCUSSION

The atomic site polarization shift model appears to do a very good job of explaining the experimental photoelectron spectra recorded by Tchapyguine *et al.*<sup>13</sup> There do remain some discrepancies which are partly model and parameter dependent. Some of the issues that we take up in turn below

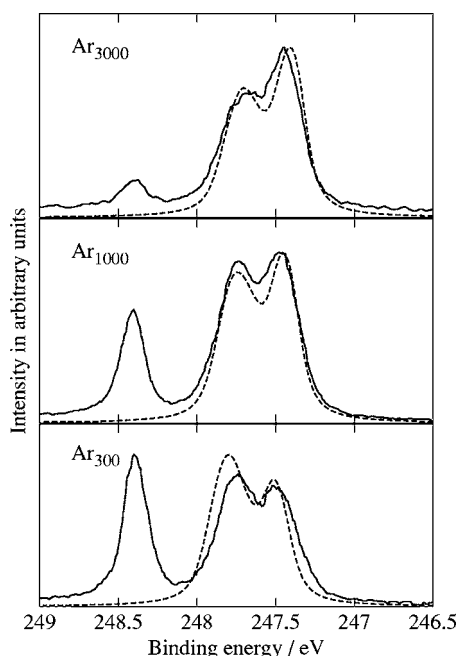


FIG. 6. Comparison of pure Ar ( $\langle N \rangle = 300, 1000, 3000$ ) experimental spectra with best fit simulated spectra ( $\lambda_{Ar} = 9.5 \text{ \AA}$ ) using clusters of size equal to the mean size. Plots are normalized to the largest cluster peak.

include the possible inadequacy of the point polarizability model, the possibility of electronic relaxation effects, the detailed procedures for preparing cluster models, and of course the uncertainty in the value of the electron attenuation length. The discrepancies in overall cluster shifts may also be partly due to the uncertainty in the mean cluster size in the experiments.

In our calculations of the polarization energy, we have attributed the same value of the point polarizability to the nascent ion as to the neutral atoms surrounding it. While the polarizability of, say,  $\text{Xe}^+$  ion is not the same as for a neutral Xe atom, the effect is small. If we were to set the polarizability of  $\text{Xe}^+$  to zero, we would observe a diminution of the polarization shift. Following the discussion of Böttcher,<sup>24</sup> we note that for a mutually polarizable ion/neutral pair a distance  $s$  apart with polarizabilities  $\alpha_1$  and  $\alpha_2$ , respectively, the polarization energy is given by

$$E_{12} = -\frac{\alpha_2 e^2}{2s^4} \frac{1}{1 - \frac{4\alpha_1 \alpha_2}{s^6}}. \quad (10)$$

For a nonpolarizable ion,  $\alpha_1 = 0$ , and so the magnitude of the shift is slightly less than for the mutually polarizable case. However, this is expected to be a small effect since, for a Xe dimer at its equilibrium distance,  $4\alpha_1 \alpha_2 / s^6 = 0.0088$ .

Turning to questions of relaxation, we note that signal electrons with 50 eV kinetic energy travel  $20 \text{ \AA}$  in about  $5 \times 10^{-16} \text{ s}$ . The Auger processes that are responsible for the electronic relaxation of the core hole, including secondary ionization, take on the order of  $5 \times 10^{-15} \text{ s}$ . This latter time scale is entirely consistent with the natural linewidths of the atomic peaks in the experimental spectra (Lorentzian full width at half maximum of  $115 \text{ meV}$ <sup>32</sup>) and so we believe that our broadening procedure has adequately accounted for

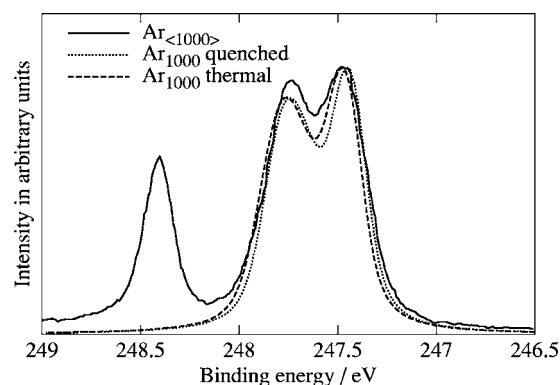


FIG. 7. Comparison of pure Ar ( $\langle N \rangle = 1000$ ) experimental spectrum with best fit simulated spectra ( $\lambda_{Ar} = 9.5 \text{ \AA}$ ) for quenched and unquenched (thermal) clusters. See text for details.

“postcollision interactions” at least to a first approximation.<sup>33</sup> The time scale for nuclear motion is about two orders of magnitude larger so the experiment and the simulation really do probe the structure of the neutral parent clusters in the beam.

We have attempted to create cluster models that mimic those found in the beam. The final temperature of the clusters cannot be ascertained directly and we have chosen to quench our models to local minimum structures before performing the polarization calculations. If the cluster models were to be maintained at finite temperatures, this would probably lead to slightly smaller binding energy shifts since, on average, the nearest neighbor shell would be slightly farther away. There might also be a small increase in the radius of the cluster and thus a change in the relative heights of the bulk and surface peaks. In Fig. 7, we reproduce the spectra of Fig. 6(b) with an additional spectrum (dashed line) calculated from the simulated clusters obtained from the end of the thermal treatment (hence at  $T = 30 \text{ K}$ ) but before quenching. We see that the nonquenched cluster spectrum is slightly less shifted and does fill in the valley between the bulk and surface peaks. However, the radius of this cluster (as determined by the procedure above) is virtually identical to the quenched cluster and leads to very similar peak heights. We will discuss another interesting effect related to temperature below.

Our cluster models have, up until now, been based on a single cluster size equal to the mean cluster sizes reported by Tchapyguine *et al.*;<sup>13</sup> these authors also report that the cluster distribution in their neutral beams has a Gaussian shape with a full width half maximum equal to the mean size  $\langle N \rangle$ . We investigated the effect of this distribution on the simulated spectrum of  $\text{Xe}_{(300)}$  by taking an average of the spectra different size clusters, weighted according to the given Gaussian probability function. There was very little net effect on the spectrum (not shown), indicating that single size models can do a pretty good job of explaining the spectra of these clusters. It is of course critical that the mean cluster size be correct: in Fig. 8 we redraw the bottom panel of Fig. 5, adding the simulated spectrum of  $\text{Xe}_{500}$  to the previous comparison of simulated spectra of  $\text{Xe}_{300}$  with the  $\text{Xe}_{(300)}$  experimental spectrum. We note that the agreement between experiment and simulation is now much better and the larger

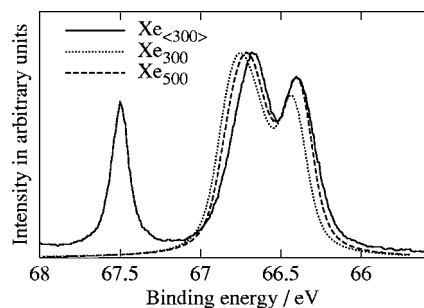


FIG. 8. Comparison of pure Xe ( $\langle N \rangle = 300$ ) spectrum with simulated spectra ( $\lambda_{Xe} = 8.5 \text{ \AA}$ ) for  $N = 300$  and  $500$ .

cluster size is close to a single  $\sigma$  uncertainty limit for the cluster distribution. Indeed this possibility is quite reasonable since Tchapyguine *et al.* point out that a “difference (in  $\langle N \rangle$ ) between 300 and 561 is within the uncertainty of the scaling law method.”<sup>13</sup>

We discuss briefly the possibility of learning more about the detailed structure of these clusters using experimental spectra whose interpretation is informed by atomic level simulation of the kind presented here. We have prepared an essentially “perfect” spherical close-packed cluster of  $Xe_{3500}$  and simulated its  $4d_{5/2}$  core-hole spectrum. This result is shown in Fig. 9 along with the simulated spectrum of Fig. 5(c). The overall width and relative peak heights of the spectrum of the perfect cluster are in reasonable accord with the earlier result (disordered cluster). In fact, we see that the leading edges of the bulk peaks are virtually the same. The interesting difference is the presence of a doublet in the surface peak. A look at this cluster shows that its surface is highly faceted and that the split surface peak is due to the different abundances of edge (or step) atoms and atoms which are entirely within a face.

## V. CONCLUSIONS

Our detailed atomistic simulations of the photoelectron spectra of Xe and Ar clusters of sizes between 300 and 3500 atoms are able to reproduce the experimental results of Tchapyguine *et al.*<sup>13</sup> The site-polarization model appears to be consistent both in shifts and intensities of the experimental observations, provided that reasonable values of the electron attenuation lengths are used. It is difficult to attribute precisely the remaining discrepancies in binding energy

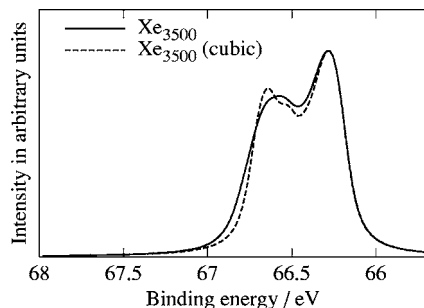


FIG. 9. Comparison of simulated  $Xe_{3500}$  spectra ( $\lambda_{Xe} = 8.5 \text{ \AA}$ ) for equilibrated cluster and a close-packed cubic starting cluster. The splitting of the surface peak in the “cubic” model is due to the highly faceted nature of the cluster.

shifts to particular factors since uncertainties in the thermal treatments we use in our MD simulations are comparable to the uncertainties in the mean size of the clusters in the beam. We plan to perform some more extensive simulations of cluster formation in an attempt to create models which are more likely to be like those in the beam. While the photoelectron spectrum appears to be much less sensitive to the packing motifs of the clusters than, for example, the electron diffraction spectrograms of Farges *et al.*,<sup>4,34</sup> one diagnostic we can use to monitor the packing arrangement of our simulated clusters is the use of local order parameters<sup>35</sup> based on the sets of angles that a 12-coordinated atom (eight-coordinated for bcc) would have under idealized packing conditions. Our procedure is related to the direction cosine distribution method discussed by Polak *et al.*<sup>36</sup>

Of greater interest is the extension of our simulation methodology to mixed rare-gas clusters, whose spectra have recently been reported. We have only undertaken some very preliminary but promising calculations so far. These will be extended and reported in a future publication. The fact that our simulations give effective attenuation lengths of  $8.5 \text{ \AA}$  and  $9.5 \text{ \AA}$  for Xe and Ar, respectively, will make the job of screening the mixed clusters easier since it is likely that some interpolated value or mole fraction weighted average value will solve the problem of determining  $\lambda$  for the Xe/Ar mixed clusters.

It may also be interesting to extend our simulation methodology to other kinds of clusters such as metals or metal oxides. For example, it would be of interest to see if the Xe core/Ar shell layering observed in Ref. 13 could be detected in metal alloy clusters like the “onionlike” layered clusters of Cu and Ag recently proposed in the simulations of Balletto *et al.*<sup>37</sup> It would also be of interest to investigate nanostructures on surfaces which may display the kind of faceting that gave rise to the split surface peak shown in Fig. 9.

## ACKNOWLEDGMENTS

The authors thank M. Lundwall for providing experimental spectra and linewidth information prior to publication, Dr. C. Powell for useful information concerning the IMFP database at NIST, and Dr. Brian Frederick for helpful discussions concerning electron attenuation.

<sup>1</sup>T. E. Gough, D. G. Knight, and G. Scoles, *Chem. Phys. Lett.* **97**, 155 (1983); F. G. Amar, S. Goyal, D. J. Levandier *et al.*, in *Clusters of Atoms and Molecules II: Solvation and Chemistry of Free Clusters, and Embedded, Supported, and Compressed Clusters*, edited by H. Haberland (Springer, Berlin, 1994), Vol. 56, p. 19; S. Goyal, G. N. Robinson, D. L. Schutt *et al.*, *J. Phys. Chem.* **95**, 4186 (1991).

<sup>2</sup>H. Vach, *Trends Chem. Phys.* **8**, 19 (2000); *J. Chem. Phys.* **111**, 3536 (1999).

<sup>3</sup>J. Farges, B. Raoult, and G. Torchet, *J. Chem. Phys.* **59**, 3454 (1973); J. Farges, M.-F. de Feraudy, B. Raoult *et al.*, *Ber. Bunsenges. Phys. Chem.* **88**, 211 (1984); G. Torchet, J. Farges, M.-F. de Feraudy *et al.*, *The Chemical Physics of Atomic and Molecular Clusters*, Proceedings of the Enrico Fermi International Summer School, edited by G. Scoles (North-Holland, Amsterdam, 1990), Vol. 107, p. 513.

<sup>4</sup>J. Farges, M. F. De Feraudy, B. Raoult *et al.*, *J. Chem. Phys.* **78**, 5067 (1983); **84**, 3491 (1986).

<sup>5</sup>J. D. Honeycutt and H. C. Andersen, *J. Chem. Phys.* **91**, 4950 (1987).

<sup>6</sup>J. Xie, J. A. Northby, D. L. Freeman *et al.*, *J. Chem. Phys.* **91**, 612 (1989).

<sup>7</sup>B. W. van de Waal, *Phys. Rev. Lett.* **76**, 1083 (1996).

- <sup>8</sup>B. W. van de Waal, G. Torchet, and M. F. de Feraudy, *Chem. Phys. Lett.* **331**, 57 (2000).
- <sup>9</sup>J. P. K. Doye and D. J. Wales, *Z. Phys. D: At., Mol. Clusters* **40**, 194 (1997).
- <sup>10</sup>D. J. Wales, *Energy Landscapes* (Cambridge University Press, Cambridge, 2003).
- <sup>11</sup>J. P. Doye and F. Calvo, *J. Chem. Phys.* **116**, 8307 (2002).
- <sup>12</sup>O. Bjorneholm, F. Federmann, F. Fossing *et al.*, *Phys. Rev. Lett.* **74**, 3017 (1995); O. Bjorneholm, *Surf. Rev. Lett.* **9**, 2 (2002); G. Ohrwall, M. Tchapyguine, M. Gisselbrecht *et al.*, *J. Phys. B* **36**, 3937 (2003); M. Tchapyguine, R. Feifel, R. R. Marinho *et al.*, *Chem. Phys.* **289**, 3 (2003).
- <sup>13</sup>M. Tchapyguine, R. R. Marinho, M. Gisselbrecht *et al.*, *J. Chem. Phys.* **120**, 345 (2004).
- <sup>14</sup>M. Lundwall, M. Tchapyguine, G. Ohrwall *et al.*, presented at the ISSPIC 11, Strasbourg, France, 2002 (unpublished).
- <sup>15</sup>M. Tchapyguine, M. Lundwall, M. Gisselbrecht *et al.*, *Phys. Rev. A* **69**, 031201 (2004).
- <sup>16</sup>R. A. Aziz, in *Inert Gases*, Springer Series in Chemical Physics, edited by M. Klein (Springer, Berlin, 1984), p. 5.
- <sup>17</sup>A. K. Dham, W. J. Meath, A. R. Allnatt *et al.*, *Chem. Phys.* **142**, 173 (1990).
- <sup>18</sup>R. A. Aziz and H. H. Chen, *J. Chem. Phys.* **67**, 5719 (1977).
- <sup>19</sup>F. Abraham, *Homogeneous Nucleation Theory: The Pretransition Theory of Vapor Condensation* (Academic, New York, 1974).
- <sup>20</sup>For Xe, our temperature/time schedule (K/ps) was (600/50) → (400/25) → (250/25) → (150/50) → (75/50) while for Ar the corresponding schedule was (350/50) → (200/25) → (125/25) → (75/50) → (30/50).
- <sup>21</sup>W. H. Press, B. P. Flannery, S. A. Teukolsky *et al.*, *Numerical Recipes: The Art of Scientific Computing* (Cambridge University Press, Cambridge, 1986).
- <sup>22</sup>D. R. Lide, *Handbook of Chemistry and Physics*, 71st ed. (CRC, Boca Raton, FL, 1990).
- <sup>23</sup>L. Perera and F. G. Amar, *J. Chem. Phys.* **89**, 7354 (1989).
- <sup>24</sup>C. J. F. Bottcher, O. C. van Belle, P. Bordewijk *et al.*, *Theory of Electric Polarization*, 2nd ed. (Elsevier Scientific, Amsterdam, 1973).
- <sup>25</sup>E. Pollock and B. Alder, *Phys. Rev. Lett.* **41**, 903 (1978).
- <sup>26</sup>A. Jablonski and C. J. Powell, *J. Electron Spectrosc. Relat. Phenom.* **100**, 137 (1999).
- <sup>27</sup>S. Tanuma, C. J. Powell and D. R. Penn, *Surf. Interface Anal.* **21**, 165 (1994).
- <sup>28</sup>S. Tougard, QUASES-IMFP-TPP2M ([http://www.quases.com/QUASES\\_IMFP\\_TPP2M/QUASES\\_IMFP\\_TPP2\\_home.htm](http://www.quases.com/QUASES_IMFP_TPP2M/QUASES_IMFP_TPP2_home.htm), 2004).
- <sup>29</sup>G. Baldini, *Phys. Rev.* **128**, 1562 (1962).
- <sup>30</sup>B. Plenkiewicz, P. Plenkiewicz, and J. P. Jay-Gerin, *Phys. Rev. B* **33**, 5744 (1986); N. Schwentner, *ibid.* **14**, 5490 (1976).
- <sup>31</sup>B. H. Armstrong, *J. Quant. Spectrosc. Radiat. Transf.* **7**, 61 (1967).
- <sup>32</sup>M. Lundwall, private communication, 2003.
- <sup>33</sup>B. Kassuhlke, R. Romberg, P. Averkamp *et al.*, *Phys. Rev. Lett.* **81**, 2771 (1998).
- <sup>34</sup>J. Farges, M. F. de Feraudy, B. Raoult *et al.*, *Jerusalem Symp. Quantum Chem. Biochem.* **20**, 113 (1987).
- <sup>35</sup>F. G. Amar and J. Smaby (unpublished).
- <sup>36</sup>W. Polak and A. Patrykiewicz, *Phys. Rev. B* **67**, 115402 (2003).
- <sup>37</sup>F. Balleto, C. Mottet, and R. Ferrando, *Phys. Rev. Lett.* **90**, 135504 (2003).
- <sup>38</sup>I. Bormann, *Digitizeit* (<http://www.digitizeit.de>, 2003).